2007

Generic nonsinusoidal phase error correction for three-dimensional shape measurement using a digital video projector

Song Zhang, *Harvard University*
Shing-Tung Yau, *Harvard University*

Generic nonsinusoidal phase error correction for three-dimensional shape measurement using a digital video projector

Song Zhang and Shing-Tung Yau

A structured light system using a digital video projector is widely used for 3D shape measurement. However, the nonlinear γ of the projector causes the projected fringe patterns to be nonsinusoidal, which results in phase error and therefore measurement error. It has been shown that, by using a small look-up table (LUT), this type of phase error can be reduced significantly for a three-step phase-shifting algorithm. We prove that this algorithm is generic for any phase-shifting algorithm. Moreover, we propose a new LUT generation method by analyzing the captured fringe image of a flat board directly. Experiments show that this error compensation algorithm can reduce the phase error to at least 13 times smaller.

OCIS codes: 120.0120, 120.2650, 120.2650, 120.5050.

1. Introduction

Optical noncontact 3D surface profile methods, including stereovision, laser scanning, and time or color-coded structured light, have been developed to obtain a 3D contour.[1,2] Structured-light-based methods have the advantage of fast 3D shape measurement and high accuracy, among which various phase-shifting methods have been widely used due to their accuracy and efficiency.[3] For phase-shifting methods, the nonsinusoidal waveform error and the phase-shift error are two major error sources.[4]

With the development of digital display technologies, commercial digital video projectors are more and more extensively utilized in 3D shape measurement systems. A structured-light-based system differs from a stereo-based system by replacing one of the cameras of the stereo system with a projector, and projects coded structured patterns, which help to identify the correspondence. The structured-light system based on a binary-coding method has the disadvantages of spatial resolution and measurement speed since the stripe width must be larger than one pixel. But it is robust to the nonlinear γ of the projector since only two levels (0s and 1s) are used for this method. In contrast, a system based on a phase-shifting method has the advantages of measurement speed and resolution because it can obtain the coordinates of the object pixel by pixel. The drawback of such a system is that it is sensitive to the nonlinear γ of the projector; any nonlinear effect deforms the ideal sinusoidal fringe pattern to be nonsinusoidal and introduces error. The phase error caused by this nonsinusoidal waveform is the single dominant error source of the measurement because the phase-shift error does not appear in this method due to the digital fringe pattern generation nature. Since any measurement error of a phase-shifting-based system will appear in the phase, similarly, the error in phase will appear in the final measurement. In this research, the measurement error due to the nonsinusoidal waveform is simply called the *phase error*. For accurate measurement, the nonlinear γ of the projector is not desirable. However, the γ of any commercial projector is purposely distorted to be nonlinear to have better visual effect. To obtain better measurement accuracy, this type of phase error has to be reduced. Previously proposed methods, including the double three-step phase-shifting algorithm,[5] 3 + 3 phase-shifting algorithm,[6,7] and direct correction of the nonlinearity of the projector's γ,[8] demonstrated significant phase error reduction; however, the residual error remains nonnegligible. Guo *et al*. proposed a γ correction

The authors are with the Department of Mathematics, Harvard University, Cambridge, Massachusetts 02138. S. Zhang's e-mail address is szhang77@gmail.com. S.-T. Yau's e-mail address is yau@math.harvard.edu.

Received 30 May 2006; revised 3 September 2006; accepted 7 September 2006; posted 11 September 2006 (Doc. ID 71457); published 15 December 2006.

0003-6935/06/010036-08$15.00/0

method using a simple one-parameter γ function technique by statistically analyzing the fringe images.[9] This technique significantly reduces the phase error due to the nonlinear γ. However, the one-parameter assumption for the γ function of the projector is too strong. The actual γ of the projector is complicated. Therefore this method cannot completely remove the error due to the projector's nonlinear γ. Skocaj and Leonardis proposed an algorithm to compensate for the nonlinear effect of the projector–camera system for range image acquisition of the objects with nonuniform albedo.[10] The algorithm works well for their purpose. However, it is time consuming to calibrate the nonlinear function, and the accuracy is not high since they did not account for the ambient light effect.

Zhang and Huang proposed a method by calibrating the γ of the projector, precomputing the phase error that is stored in a look-up table (LUT), which was used to reduce the phase error significantly for a three-step phase-shifting algorithm.[11] In this research we prove that this type of phase error compensation method is not limited to the three-step phase-shifting method. It is generic for any phase-shifting method. The phase error compensation algorithm is able to theoretically eliminate the phase error caused by the projector's γ completely. It is based on our finding that, in the phase domain, the phase error due to the γ of the projector is preserved for the arbitrary object's surface reflectivity under an arbitrary ambient lighting condition. However, the method introduced by Zhang and Huang requires calibration of the projector's γ, which is a time-consuming procedure. Moreover, it requires the projectors γ to be monotonic, so that the phase error LUT can be created. In this research, we propose a method that does not require calibration of the γ of the projector directly and does not require the γ to be monotonic. Instead, we use a calibration board, image it, and analyze the fringe images to obtain the phase error LUT. A uniform flat surface is utilized for such a purpose. We captured a set of fringe images of a uniform flat surface board. The phase error of the captured fringe images is analyzed and stored in a LUT for phase error compensation. This method is also suitable for use in other phase-shifting-based systems when the nonlinearity of the fringe generator is difficult to obtain. Therefore it is more general than the previously proposed method. Our experimental results show that, by using this method, the measurement error can be reduced by at least 13 times for any phase-shifting algorithm.

In Section 2 we explain the theoretical background of this error compensation method. In Section 3 we explain the LUT creation procedures. Section 4 shows the experimental results. Section 5 discusses the advantages and limitations of the method, and Section 6 concludes the paper.

2. Principle

A. Least-Squares Algorithms

The phase-shifting method has been adopted extensively in optical metrology to measure 3D shapes of objects at various scales. Many different sinusoidal phase-shifting algorithms have been developed; the general form of phase-shifting algorithms is the least-squares algorithms. The intensity of the ith images with a phase shift of δ_i is as follows:

$$I_i(x, y) = I'(x, y) + I''(x, y)\cos(\phi(x, y) + \delta_i), \quad (1)$$

where I' is the average intensity, I'' is the intensity modulation, and ϕ is the phase to be solved.

Solving Eq. (1) simultaneously by the least-squares algorithm, we obtain

$$\phi(x, y) = \tan^{-1}\left(\frac{-a_2(x, y)}{a_1(x, y)}\right), \quad (2)$$

$$\gamma(x, y) = \frac{I''(x, y)}{I'(x, y)} = \frac{[a_1(x, y)^2 + a_2(x, y)^2]^{1/2}}{a_0(x, y)}, \quad (3)$$

where

$$\begin{bmatrix} a_0(x, y) \\ a_1(x, y) \\ a_2(x, y) \end{bmatrix} = \mathbf{A}^{-1}(\delta_i)\mathbf{B}(x, y, \delta_i). \quad (4)$$

Here,

$$\mathbf{A}(\delta_i) = \begin{bmatrix} N & \sum\cos(\delta_i) & \sum\sin(\delta_i) \\ \sum\cos(\delta_i) & \sum\cos^2(\delta_i) & \sum\cos(\delta_i)\sin(\delta_i) \\ \sum\sin(\delta_i) & \sum\cos(\delta_i)\sin(\delta_i) & \sum\sin^2(\delta_i) \end{bmatrix}, \quad (5)$$

$$\mathbf{B}(x, y, \delta_i) = \begin{bmatrix} \sum I_i \\ \sum I_i\cos(\delta_i) \\ \sum I_i\sin(\delta_i) \end{bmatrix}, \quad (6)$$

where $I'(x, y) = a_0(x, y)$ can be used to obtain the flat image of the measured object. Equation (2) provides the so-called modulo 2π phase at each pixel, whose values range from 0 to 2π. If a multiple fringe pattern is used, a continuous phase map can be obtained by phase unwrapping.[12] The continuous phase map can be further converted to coordinates through calibration.[13,14]

B. Phase Error Correction

The images captured by the camera are formed through the procedures illustrated in Fig. 1. Let us

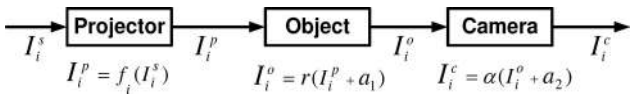

Fig. 1. Camera image generation procedure.

assume that the projector's input sinusoidal fringe images generated by a computer have intensity

$$I_i^s(x, y) = b_1\{1 + \cos[\phi(x, y) + \delta_i]\} + b_0, \quad (7)$$

where b_1 is the dynamic range of the fringe images and b_0 is the bias. After being projected by the projector, the output intensity of the fringe images becomes

$$I_i^p(x, y) = f_i(I_i^s), \quad (8)$$

where $f_i(I_i^s)$ is a function of I_i^s, which represents the real projection response of the projector to the input intensity for the ith image, the γ. If we assume that the projector projects light onto a surface with reflectivity $r(x, y)$ and the ambient light $a_1(x, y)$, the reflected light intensity is

$$I_i^o(x, y) = r(x, y)[I_i^p(x, y) + a_1(x, y)], \quad (9)$$

The reflected image is captured by a camera with a sensitivity of α, here we assume the camera is the linear response to the input light intensity, namely, α is a constant. Then, the intensity of the image captured by the camera is

$$I_i^c(x, y) = \alpha[I_i^o + a_2(x, y)], \quad (10)$$

$$= \alpha r(x, y) I_i^p + \alpha r(x, y) a_1(x, y) + \alpha a_2(x, y), \quad (11)$$

$$= c_1 I_i^p + c_2, \quad (12)$$

where $a_2(x, y)$ represents ambient light entering the camera. $c_1 = \alpha r(x, y)$ and $c_2 = \alpha r(x, y) a_1(x, y) + \alpha a_2(x, y)$.

If we assume

$$\mathbf{C} = \mathbf{A}^{-1} = \begin{bmatrix} C_{00} & C_{01} & C_{02} \\ C_{10} & C_{11} & C_{12} \\ C_{20} & C_{21} & C_{22} \end{bmatrix}, \quad (13)$$

then

$$a_2(x, y) = C_{20} \sum I_i^c + C_{21} \sum I_i^c \cos(\delta_i) + C_{22} \sum I_i^c \sin(\delta_i), \quad (14)$$

$$= C_{20} \sum (c_1 I_i^p + c_2) + C_{21} \sum (c_1 I_i^p + c_2) \times \cos(\delta_i) + C_{22} \sum (c_1 I_i^p + c_2) \sin(\delta_i), \quad (15)$$

$$= c_1[C_{20} \sum I_i^p + C_{21} \sum I_i^p \cos(\delta_i) + C_{22} \sum I_i^p \sin(\delta_i)] + C_2[C_{20} N + C_{21} \sum \cos(\delta_i) + C_{22} \sum \sin(\delta_i)]. \quad (16)$$

From $\mathbf{C} = \mathbf{A}^{-1}$, i.e., $\mathbf{CA}$ = identity. From Eqs. (5) and (13) for definition of matrices $\mathbf{A}$ and $\mathbf{C}$, the third row, first column element in the resultant matrix is zero, we have

$$C_{20} N + C_{21} \sum \cos(\delta_i) + C_{22} \sum \sin(\delta_i) = 0.$$

If we substitute these constraints into Eq. (16), we obtain

$$a_2(x, y) = c_1[C_{20} \sum I_i^p + C_{21} \sum I_i^p \cos(\delta_i) + C_{22} \sum I_i^p \sin(\delta_i)]. \quad (17)$$

Similarly, we can prove that

$$a_1(x, y) = c_1[C_{10} \sum I_i^p + C_{11} \sum I_i^p \cos(\delta_i) + C_{12} \sum I_i^p \sin(\delta_i)]. \quad (18)$$

From Eq. (2), phase $\phi(x, y)$ is

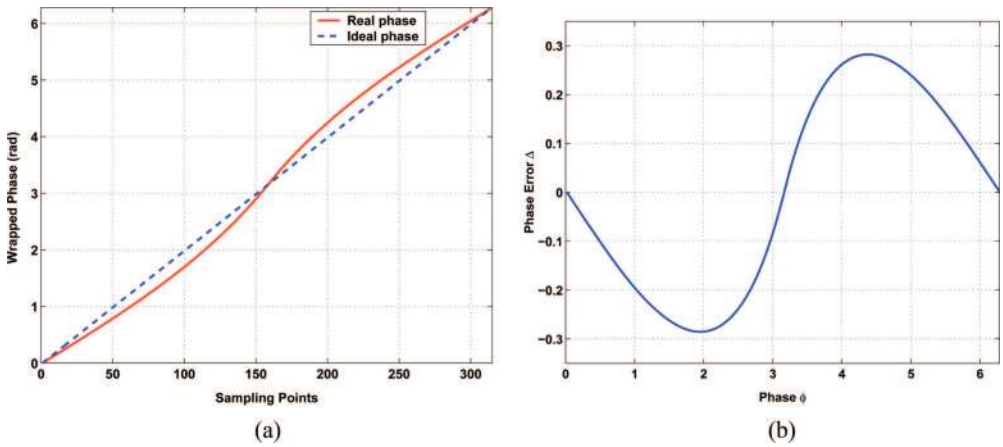

Fig. 2. (Color online) Phase error LUT generation. (a) Real wrapped phase and the ideal wrapped phase. (b) Phase error relative to the real wrapped phase.

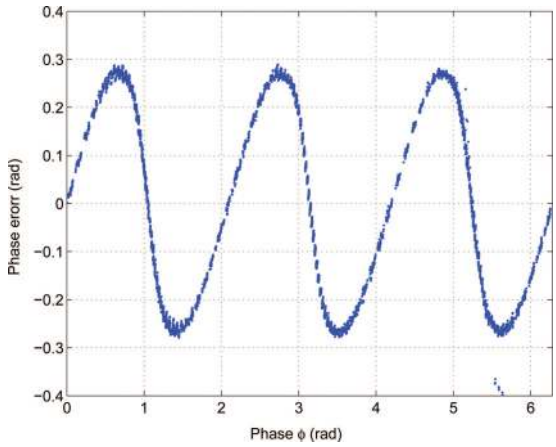

Fig. 3. (Color online) Phase error with a fringe pitch of 120.

However, once the fringe images are distorted to be nonsinusoidal due to the nonlinear effects of the system, e.g., the γ of the projector, the real wrapped phase $\phi(x, y)$ is nonlinear. The difference between the wrapped phase and the ideal linear one is

$$\Delta(\phi(x,\ y)) = \phi(x,\ y) - kx. \tag{22}$$

Here $k = 2\pi/N$ is the slope of the line ranging from 0 to 2π; N is the number of points sampled in one fringe period. Δ is a function of the computed real phase value $\phi(x, y)$. The error LUT is therefore constructed as a map (ϕ, Δ). Figure 2 shows the phase error creation method. In this figure, we used 312 sampling points to show the concept. Figure 2(a) plots the real wrapped phase values and the ideal phase values for each sampling point. We subtract the real phase value by the ideal phase value for each point and obtain its phase error. The phase error corresponding to the real wrapped phase value is plotted in Fig. 2(b). Once the discrete values of phase errors are obtained for the corresponding phase, the continuous phase error map can be obtained by fitting the data with splines. The error LUT can then be created by sampling the spline curve and storing the value in a LUT.

$$\phi(x,\ y) = \tan^{-1}\left\{\frac{-a_2(x,\ y)}{a_1(x,\ y)}\right\}, \tag{19}$$

$$= \tan^{-1}\left\{\frac{-c_1\left[C_{20}\sum I_i^p + C_{21}\sum I_i^p \cos(\delta_i) + C_{22}\sum I_i^p \sin(\delta_i)\right]}{c_1\left[C_{10}\sum I_i^p + C_{11}\sum I_i^p \cos(\delta_i) + C_{12}\sum I_i^p \sin(\delta_i)\right]}\right\}, \tag{20}$$

$$= \tan^{-1}\left\{\frac{-C_{20}\sum I_i^p + C_{21}\sum I_i^p \cos(\delta_i) + C_{22}\sum I_i^p \sin(\delta_i)}{C_{10}\sum I_i^p + C_{11}\sum I_i^p \cos(\delta_i) + C_{12}\sum I_i^p \sin(\delta_i)}\right\}. \tag{21}$$

From Eqs. (19)–(21) we can see that phase $\phi(x, y)$ is independent of the response of the camera, the reflectivity of the object, and the intensity of the ambient light. This indicates that the phase error due to nonsinusoidal waveforms depends only on the nonlinearity of the projector's γ. Therefore if the projector's γ is calibrated, and the phase error due to the nonlinearity of the γ is calculated, a LUT that stores the phase error can be constructed for error compensation, since the wrapped phase $\hat{\phi}(x, y)$ for the ideal sinusoidal fringe images with vertical stripes increases linearly from 0 to 2π horizontally within one period.

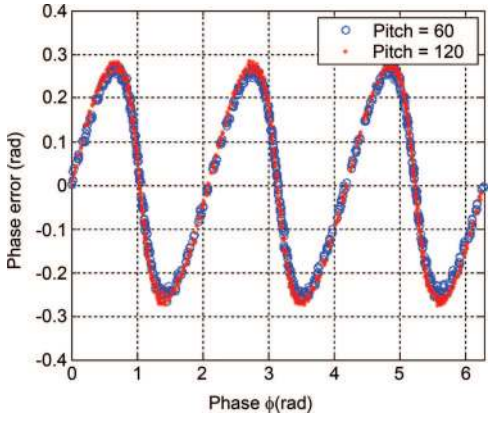

Fig. 4. (Color online) Phase error for fringe pitches 60 and 120.

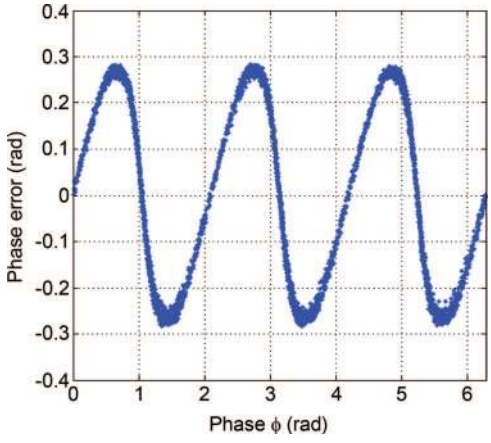

Fig. 5. (Color online) Phase error for multiple fringe pitches (Pitch = $60 + 30 \times k$, $k = 1, 2, \ldots, 6$).

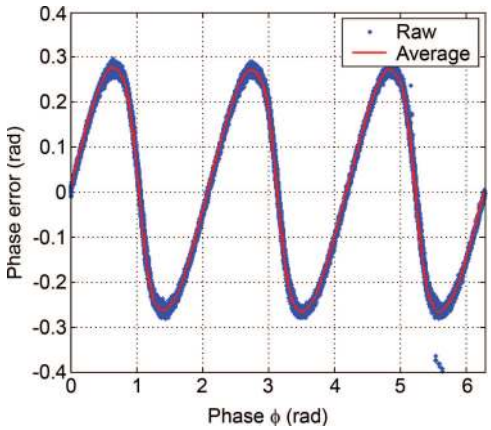

Fig. 6. (Color online) Phase error LUT creation.

3. Look-Up-Table Generation

Zhang and Huang proposed a phase error LUT generation method by calibrating the γ of the projector, precomputing the phase error value for the corresponding phase value, and storing them in a LUT.[11] They demonstrated that the proposed method can reduce the error to ten times smaller. However, this method requires calibration of the projector's γ, which is a time-consuming procedure. Moreover, it requires the projector's γ to be monotonic, so that the phase error LUT can be created. In this research, we propose a method that does not require the calibration of the γ of the projector directly and does not require the γ to be monotonic. Instead, we use a calibration board, image it, and analyze the fringe images to obtain the phase error LUT. A uniform flat surface is utilized for such a purpose.

To study the characteristics of the phase error, we project four phase-shifted fringe patterns with an arbitrary phase shift of $\delta_1 = 0°$, $\delta_2 = 270°$, $\delta_3 = 130°$, and $\delta_4 = 220°$ onto the calibration board, capture the images using the camera, and compute the phase error using the method introduced in the previous section. The phase error is shown in Fig. 3. In this figure, the fringe pitch, the number of pixels per fringe period, used is 120. We used ten-row points in the center of the image. It can be clearly seen that the phase error is a pattern similar to the phase.

We further analyze the phase error using two different fringe pitches, 60 and 120, respectively. The phase errors of ten rows on different points from the center of the image are shown in Fig. 4. It can be seen that for different fringe pitches, the phase error pattern is also similar. From Fig. 4 we can also see that the phase error is independent of the projected fringe pitch. To verify this, we image the same board and obtain the phase error from a series of fringe image sets for different fringe pitches. The result is shown in Fig. 5. The fringe pitch numbers used in this experiment range from 60 to 240 within intervals of 30. This figure shows that the phase error pattern is well maintained for different fringe pitches. These experiments demonstrated that the phase error is independent of the fringe pitch number used in the measurement. Therefore the phase error LUT can be built based on one pitch fringe image set.

In this research we use the fringe pitch of 120 as an example to create the LUT. We project four fringe images with the same phase shift as previously specified onto a uniform flat board, capture them, and compute the phase error. Figure 6 plots the phase error for 101 row points. The phase error map can then be quantized and stored in a LUT. Let us assume that we want to create a 256-element error LUT. We then divide the 2π period into 256 regions. For the kth region, the phase value ranges from $(k - 1)2\pi/256$ to $k2\pi/256$. The average error of the data points that belong to this region is stored in the kth element of the LUT. The solid curve in Fig. 6 plots the errors stored in the LUT. Once the phase error LUT is created, it can be used for future error compensation. For real captured fringe images, the phase computed from the fringe images can then be compensated for by using this LUT. Assume the phase value for one point is ϕ_0, which belongs to region $k_0 = [256\phi_0/2\pi]$, here the operator $[x]$ provides the rounded integer value of x. Then, the compensated phase is $\phi' = \phi_0 - \mathrm{LUT}(k_0)$.

4. Experimental Results

To demonstrate the performance of the proposed phase error compensation algorithm, we built a 3D shape measurement system using a digital video projector (Optoma EP739) and a CCD digital camera (Dalsa CA-D6-0512). The digital video projector projects four phase-shifted fringe images with phase shifts of $\delta_1 = 0°$, $\delta_2 = 270°$, $\delta_3 = 130°$, and $\delta_4 = 220°$, the CCD camera captures the reflected

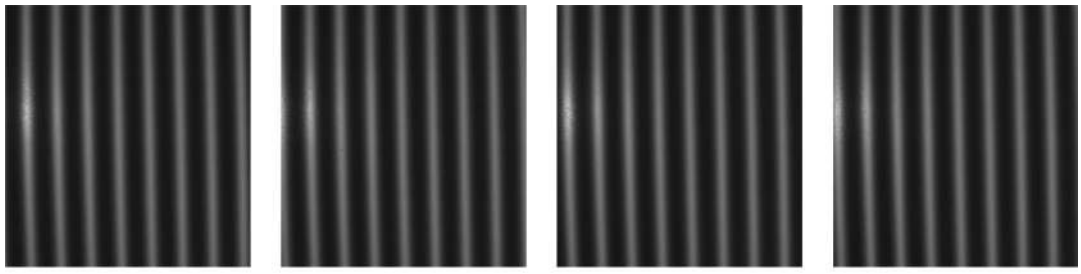

Fig. 7. Phase-shifted fringe images for the flat board: (a) I_1 ($\delta_1 = 0°$), (b) I_2 ($\delta_2 = 270°$), (c) I_3 ($\delta_3 = 130°$), (d) I_4 ($\delta_4 = 220°$).

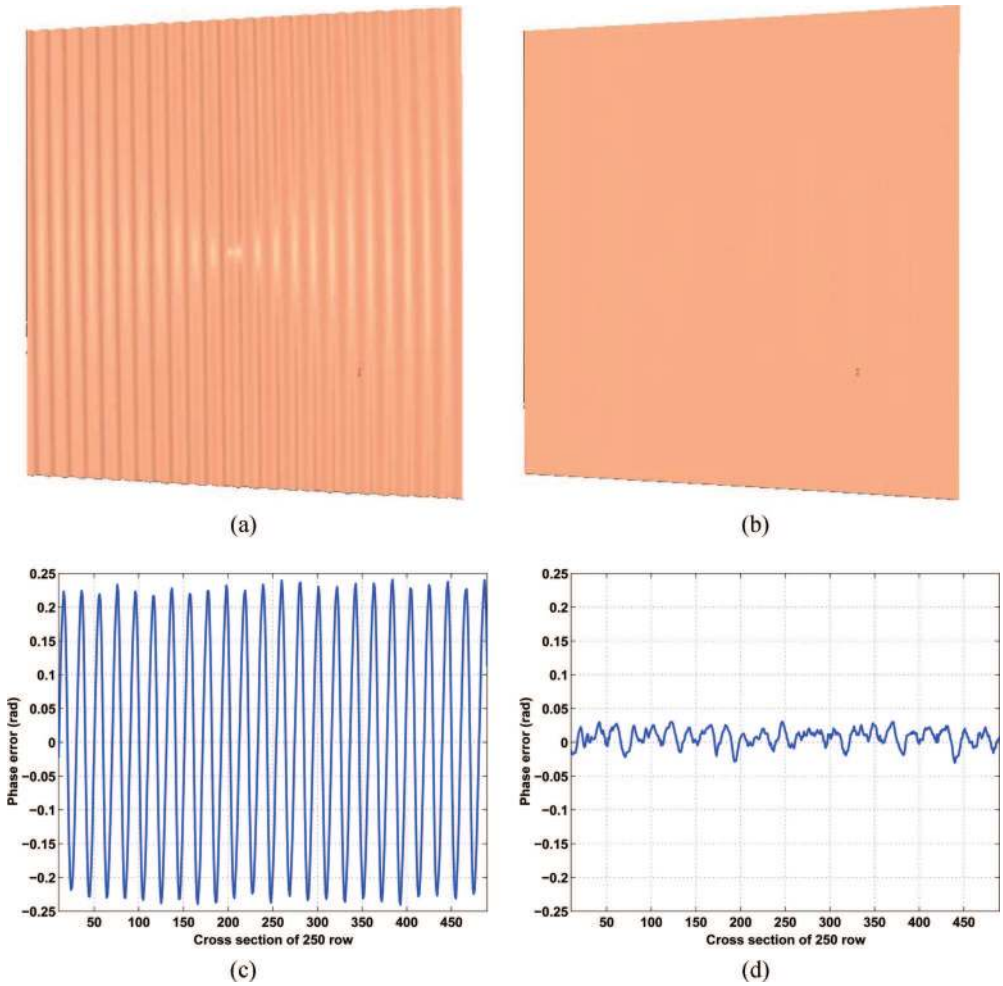

Fig. 8. (Color online) Three-dimensional measurement result of flat board before and after error compensation. (a) Three-dimensional geometry without correction. (b) Three-dimensional geometry after correcting the phase. (c) Cross section of the 250th row of the above image (rms: 0.16 rad). (d) Cross section of the 250th row of the above image (rms: 0.02 rad).

fringe images by the object. Figure 7 shows all the fringe images of the flat board. Figure 8 shows the 3D measurement results before and after phase error correction. The phase error before error reduction is approximately rms 0.16 rad and reduces to rms 0.012 rad once the phase error compensation algorithm is applied. The error is approximately 13 times smaller.

We also implemented the error compensation algorithm in our real-time 3D shape system using a three-step phase-shifting method.[15–17] Figure 9 shows the measurement results of the flat board using the algorithm proposed in this paper and the one developed in Ref. 11. In comparison with the previously proposed method, the error compensation method proposed here is much simpler and faster, since no

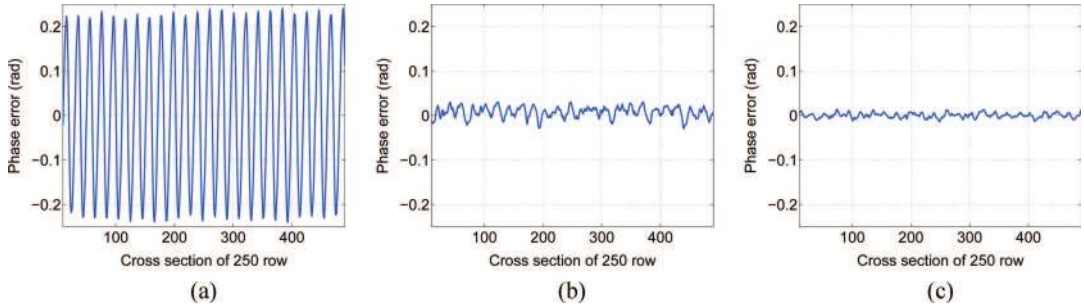

Fig. 9. (Color online) Comparison of the proposed method and the method developed in Ref. 11. (a) Phase error before compensation (rms: 0.16 rad). (b) Phase error after error compensation with the algorithm proposed in this paper (rms: 0.012 rad). (c) Phase error after error compensation using the previously proposed algorithm (rms: 0.006 rad).

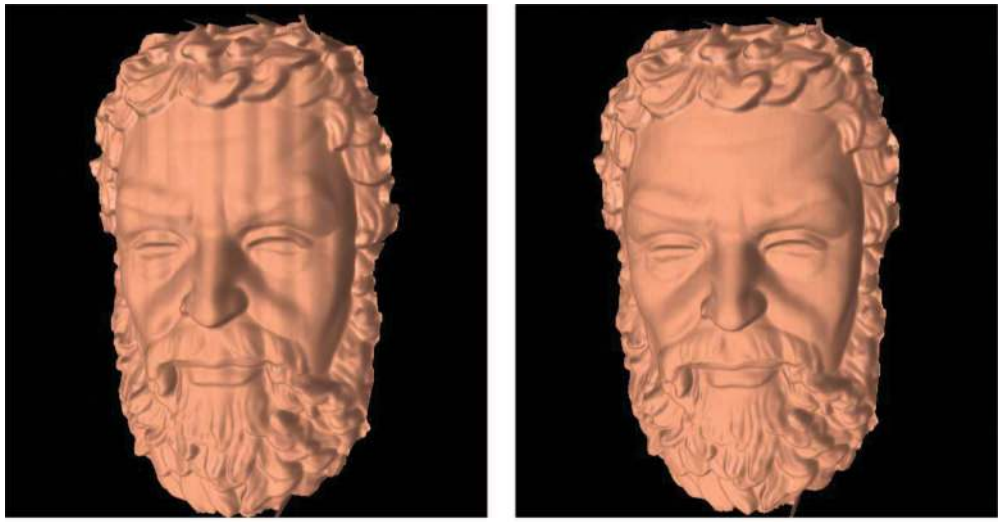

(a) (b)

Fig. 10. (Color online) Three-dimensional measurement results of a sculpture (a) before and (b) after error compensation.

projector's γ calibration is required, although its accuracy is mitigated.

In addition, we measured a more complex plaster model, Zeus's head. Figure 10 shows the reconstructed 3D models before and after error compensation. The reconstructed 3D geometric surface after error compensation is much smoother and has better visual effects. These experimental results confirm that the error correction algorithm successfully improved the accuracy of measurement significantly.

5. Discussions

The phase error compensation method discussed in this paper has the following advantages:

- *Simple*. The compensation algorithm is simple since the phase error can be easily corrected using a small LUT.
- *Accurate*. In theory, the phase error due to a nonlinear γ curve can be completely eliminated as long as the projection response functions can be determined accurately by calibration.
- *Universal*. The method discussed can correct the phase errors due to the nonsinusoidal waveform for any phase-shifting algorithm and for any system using a phase-shifting-based method.

On the other hand, the algorithm is based on the assumption that the camera is a linear device. This assumption is true for most of the cameras, although some cameras may be nonlinear. If the camera is nonlinear, it has to be calibrated before applying this algorithm.

6. Conclusions

We have introduced an error compensation method for the 3D shape measurement system using a digital video projector. We proved that the phase error caused by the nonlinear γ of the projector can be theoretically completely eliminated for any phase-shifting algorithm. It is based on our finding that the phase error caused by the projector's nonlinear γ is preserved for the arbitrary object's surface reflectivity under an arbitrary ambient lighting condition. A simple phase error LUT creation method was introduced that uses a uniform calibration board and fringe image analysis technique. The experimental results demonstrated that by utilizing a small LUT (256 elements in this research), the phase error can be reduced to at least 13 times smaller. Theoretical analysis and experimental findings were also presented.

This work was supported by Geometric Informatics, Inc., funded by the Advanced Program Project (ATP) of the National Institute of Standards and Technology (NIST).

References

1. J. Davis, R. Ramamoorthi, and S. Rusinkiewicz, "Spacetime stereo: a unifying framework for depth from triangulation," IEEE Trans. Pattern Anal. Mach. Intell. **27,** 1–7 (2005).
2. J. Salvi, J. Pages, and J. Batlle, "Pattern codification strategies in structured light systems," Pattern Recogn. **37,** 827–849 (2004).
3. D. Malacara, ed., *Optical Shop Testing* (Wiley, 1992).
4. K. Hibino, B. F. Oreb, D. I. Farrant, and K. G. Larkin, "Phase shifting for nonsinusoidal waveforms with phase-shift errors," J. Opt. Soc. Am. A **12,** 761–768 (1995).
5. P. S. Huang, Q. Hu, and F.-P. Chiang, "Double three-step phase-shifting algorithm," Appl. Opt. **41,** 4503–4509 (2002).
6. J. Schwider, R. Burow, K.-E. Elssner, J. Grzanna, R. Spolaczyk, and K. Merkel, "Digital wave-front measuring interferometry: some systematic error sources," Appl. Opt. **22,** 3421–3432 (1983).
7. J. C. Wyant and K. N. Prettyjohns, "Optical profiler using improved phase-shifting interferometry," U.S. patent 4,639,139 (27 January 1987).
8. P. S. Huang, C. Zhang, and F.-P. Chiang, "High-speed 3-D shape measurement based on digital fringe projection," Opt. Eng. **42,** 163–168 (2003).

9. H. Guo, H. He, and M. Chen, "Gamma correction for digital fringe projection profilometry," Appl. Opt. **43,** 2906–2914 (2004).
10. D. Skocaj and A. Leonardis, "Range image acquisition of objects with nonuniform albedo using structured light range sensor," in *Proceedings of the International Conference on Pattern Recognition* (IEEE, 2000), Vol. 1, pp. 778–781.
11. S. Zhang and P. S. Huang, "Phase error compensation for a 3-D shape measurement system based on the phase-shifting method," in *Two- and Three-Dimensional Methods for Inspection and Metrology III,* K. G. Harding, ed., Proc. SPIE **6000,** 133–142 (2005).
12. D. C. Ghiglia and M. D. Pritt, *Two-Dimensional Phase Unwrapping: Theory, Algorithms, and Software* (Wiley, 1998).
13. R. Legarda-Sáenz, T. Bothe, and W. P. Jüptner, "Accurate procedure for the calibration of a structured light system," Opt. Eng. **43,** 464–471 (2004).
14. S. Zhang and P. S. Huang, "Novel method for structured light system calibration," Opt. Eng. **45,** 083601 (2006).
15. S. Zhang and P. Huang, "High-resolution, real-time 3-D shape acquisition," in *IEEE Computer Vision and Pattern Recognition Workshop* (CVPRW) on Real-Time 3D Sensors and Their Uses (IEEE, 2004), Vol. 3, pp. 28–37.
16. S. Zhang and P. S. Huang, "High-resolution, real-time 3-D shape measurement," Opt. Eng., to be published.
17. S. Zhang and S.-T. Yau, "High-resolution, real-time absolute coordinate measurement based on the phase shifting method," Opt. Express **14,** 2644–2649 (2006).